FULL PAPER

steel
research
international

www.steel-research.de

Check for updates

Strain Hardening Dependence on the Structure in Dual-Phase Steels

Mohamed Soliman* and Heinz Palkowski

Herein, an extensive study is presented on the microstructure–tensile properties relationship in dual-phase (DP) steels. A series of ferrite-martensite DP steels with varied martensite volume fractions (V_m) from 0.17 to 0.86, microstructure morphologies (globular and elongated) and structure finenesses (ferrite grain sizes from 1.9 to 10.7 μm) are produced applying appropriate heat treatments. The tensile properties are studied, and the strain hardening behavior is analyzed in terms of Holloman, Crussard–Jaoul (C–J) and modified C–J approaches. The tensile curves reveal up to three strain hardening stages with the highest strain hardening exponent at the beginning of straining. Increasing V_m and refining the structure raises the number of strain hardening stages and improves the strain hardening capacity in the first stage (n_1). For the DP steels with similar morphologies, the mean free path in ferrite (λ_f) is proposed to be the most significant microstructure factor affecting n_1-value. The n_1 of the elongated morphology shows stronger dependence on λ_f than the globular one. Finally, the DP steels are subjected to aging treatments, which lead to improved yield strength and total elongation, however, the strain hardening exponent decreases significantly.

1. Introduction

Advanced high strength steels (AHSS) is a family of steels finding increased applications in automotive industry because they help to meet the tightened regulations on lower emissions while improving crash worthiness in a cost-effective manner. This steel group mainly includes dual-phase (DP) steels, transformation induced plasticity (TRIP), quenching-partitioning (Q&P),

complex-phase (CP), and twinning induced plasticity (TWIP) steels. DP steels, whose microstructure consists of a ferrite matrix and a second hard phase of martensite or bainite, are widely utilized in automotive industry, especially in passenger cars due to their superior combination of strength and ductility, better weldability, and relatively simple processing route.[1,2] Their application is constantly growing in automotive industry; e.g., it increased from 12% in the 2003 GM models to reach 36% in recent models, making this the most commonly used steels in the current products. No DP steels were used in GM models of the 1990s.[2] Indeed, the start of developing and characterization of this steel grade dates back to the end of 1970s and beginning of 1980s by privileged efforts of researchers like Davies et al.,[3,4] Gladman et al.,[5,6] and Sarosiek et al.[7,8] with studies presenting the basis for developing and comprehending the characteristics of the recent grades of this retrieved industrially valuable steel.

DP steels can be processed to different mechanical characteristics by varying the volume fractions of the constituent phases, their distribution, morphologies, and grain sizes.[9–15] Karimi and Kheirandish concluded that the DP steels having ferrite and bainite phase microstructure possess more ductility and higher work hardening exponent, whereas those with ferrite–martensite microstructure show higher ultimate tensile and yield strength.[12] The dependence of the DP steel strength on the martensite volume fraction (V_m) is a matter of debate in the literature. Many authors showed a linear increase in yield and tensile strength by increasing V_m[2,3,13,16] others posited about 0.5 as the optimal V_m at which the strength is at its peak.[15,17] On the other hand, Sun et al.[18] showed that the yield-to-tensile strength ratio is reduced when the content of ferrite increases. Bag et al. illustrated that the DP steel having dispersed martensite distribution shows better impact toughness and ductility than the one with a banded microstructure.[15] Sun and Pugh showed that the mechanical properties of DP steels not only depend on the martensite fraction and its distribution but also on its morphology; they illustrated that DP steels with elongated martensite "fiber" show increased strengths but lowers their ductility.[19] The martensite cracks more easily in fibrous martensite than in a blocky one.[20] Moreover, Kim and Nakagawa concluded that the fine fibrous DP structure produced by intermediate quenching has a much higher ductile-to-brittle transition temperature (DBTT) than the fine globular structure produced by intercritical

Dr. M. Soliman, Prof. H. Palkowski
Institute of Metallurgy
Clausthal University of Technology
Robert-Koch-Straße 42, 38678 Clausthal-Zellerfeld, Germany
E-mail: mohamed.soliman@tu-clausthal.de

Dr. M. Soliman
Faculty of Engineering
Galala University
43511 Galala City, Egypt

The ORCID identification number(s) for the author(s) of this article can be found under https://doi.org/10.1002/srin.202000518.

ADVANCED
SCIENCE NEWS
www.advancedsciencenews.com

steel
research
international

www.steel-research.de

annealing, regardless of the volume fraction of martensite.[21] The martensite morphology affects also the strain hardening capacity; the DP steels with fibrous martensite exhibit less strain hardening than that ones with blocky martensite.[20]

Being a polycrystalline material, DP steels show a considerable enhancement of strength with refining its grain size. Peng-Heng and Preban reported that the effect of ferrite grain size on the yield strength is much stronger than the one on the tensile strength.[22] In addition, refining the DP steel is shown to be effective in increasing the initial strain hardening rate.[14,23,24] Also, Calcagnotto et al. concluded that the impact toughness is improved by grain refinement, which is revealed by a lower DBTT and an increase in both upper and lower shelf energy.[14]

The previous delineation of researchers attempted to study the inter-relationship between microstructural variables and mechanical properties of DP steels, suggesting that the efforts mainly relay on varying the martensite volume fraction and/or refining the ferrite grain size in the DP steel microstructure.[2,3,13,14,16,17,24,25] Very limited literature is reported to investigate the effect of changing the structure morphology.[15,20] Some of the literature studied separate microstructure parameters,[3,13,14,16,24] whereas others combined varying the martensite volume fraction with varying structure morphology[15,20] or with varying the grain size.[26] The objective of this study is to acquire an understanding of the interplay among the three microstructural parameters: phase fraction, structure morphology, and structure fineness on tensile properties of DPs steel with a focus on strain hardening behavior. In the current investigation 13 DP steels with varying microstructural characteristics but same chemical composition were produced by applying designed heat treatments to vary the martensite fraction, structure size, and morphology.

2. Experimental Section

2.1. As-Received Material and Samples Preparation

A 2 mm industrially produced hot rolled DP sheet with 0.075 wt% C, 1.02 wt% Mn, and 0.43 wt% Cr was used as a primary material for the production of DP steels with different microstructure characteristics. Standard subsize tensile specimens with 6.4 mm width and 25.4 mm gage length were machined in accordance to ASTM standard E8-03.[27] The specimens were machined in the rolling direction.

2.2. Heat Treatments

Throughout this study, the microstructural characteristics were varied by applying different heat-treatment cycles with the aim of providing an insight into the effect of phase fraction, grain size and morphology on the mechanical behavior of the DP steel. The heat treatment procedures used to produce the aforementioned microstructures were designed using a combination of physical simulation via dilatometry, and thermodynamic simulation using the ThermoCalc software.[13] Finally, the dilatometer was used to investigate the thermal cycle required to produce the aforementioned microstructures before moving to the production of the large-scale tensile samples. The means to produce the different microstructures are schematically shown in **Figure 1**. The microstructure characteristics were varied as follows: 1) Phase fraction: this was changed by changing the intercritical annealing temperature (T_i), up to six intercritical austenitization temperatures were investigated. 2) Martensite morphology: the effect of changing the grain morphology into a lamellar one was investigated by fully austenitizing specimens at 920 °C and water quenching to create a fully martensitic structure. The samples then were intercritically annealed and quenched to produce the required final martensite amounts. Specimens that underwent this treatment are designated as "M2." The granular microstructure morphology is designated as "M1." 3) Grain size: the effect of varying grain size was investigated by producing a DP steel with larger grain size. This is achieved by austenitizing the specimens at 1000 °C for 20 min, to allow the prior austenite grains to grow, followed by cooling to and holding in the intercritical region, then quenching. Specimens that underwent this treatment are designated as "G2." The direct intercritically annealed microstructure is designated by "G1."

Accordingly, a designation system was used to indicate the microstructures resulting from different treatments, three different modifications were studied. G1M1 indicates granular morphology (M1) in smaller grain size (G1), G1M2 indicates the smaller grain size but with lamellar morphology (M2), and G2M1 indicates a granular morphology with a larger grain size (G2).

2.3. Microstructure Characterization

After salt bath treatments, specimens were sectioned perpendicular to the width direction, mounted, ground, and polished
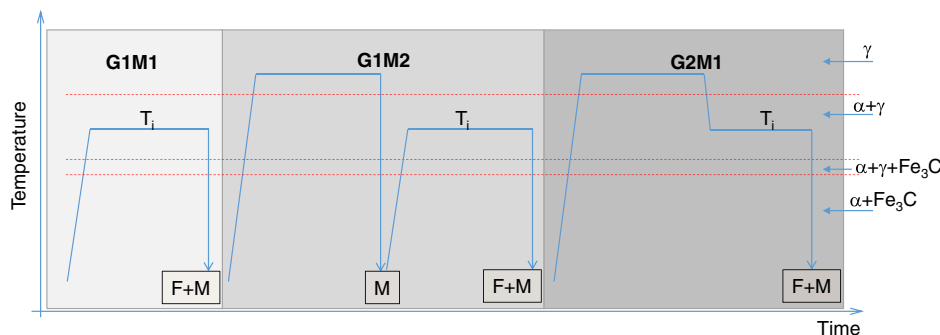

Figure 1. Schematic of the applied heat treatments to produce the different conditioned material groups with varied microstructure characteristics (F: ferrite and M: martensite).

before Nital etching. Phase analysis was carried out on photomicrographs of the light optical microscope (LOM) and scanning electron microscope (SEM). Stereological measurements were carried out to evaluate: 1) the volume fraction of martensite (V_m) using the manual point count method.[28] 2) the ferrite grain size (d_f) and martensite particle size (d_m) applying the linear intercept method.[29] 3) the mean free path in ferrite (λ_f), where λ_f represents the average lineal distance in ferrite without encountering an obstacle (here the martensite phase). This spacing is easily assessed by counting the number of martensitic particles intercepted per unit length of test line (N_L), without measuring any spacing, using the equation[30]:

$$\lambda_f = (1 - V_m)/N_L \qquad (1)$$

2.4. Tensile Testing

A 25 ton computerized universal testing machine equipped with a video extensometer was used for conducting the tensile test until fracture. Three separate tensile tests were carried out for each steel. For accurate identification of the yield points, a slow strain rate of $0.00025\,\mathrm{s}^{-1}$ was applied during the yielding stage, after yielding a strain rate of $0.0067\,\mathrm{s}^{-1}$ was applied until fracture.[27]

2.5. Aging

To examine the effect of aging on the tensile behavior, selected treated DP steels were aged in an air circulated oven at $170\,^\circ$C for 20 min. The termination of the aging process was accomplished by quenching the samples in water.

3. Results and Discussions

3.1. Microstructure Features

The intercritical annealing was carried out by heating the tensile samples up to T_i before quenching in brine to room temperature (RT). Different intercritical annealing temperatures were selected based on the ThermoCalc calculations, using the database TCFE8. According to dilatometric measurements carried out on this steel, the temperature range of the intercritical region lays between $Ae_1 = 702\,^\circ$C and $Ae_3 = 854\,^\circ$C.[13]

Representative LOM micrographs of the three conditioned materials groups G1M1, G1M2, and G2M1 are shown in **Figure 2**. The SEM micrographs of G1M1 and G1M2 microstructures are shown in **Figure 3** and those of G1M2 are shown in **Figure 4**. The morphological distributions of the constituent phases of G1M1 and G2M1 DP steels exhibit well-distributed blocky characteristics, see Figure 2 and 3. The microstructural characteristics G1M2-DP steels are not distinguishable using the LOM micrographs in Figure 2. The SEM micrographs of Figure 4 show that the ferritic regions in the G1M2 specimens are distinguished by an elongated form with nondistinctive directionality. They are encapsulated by dispersed globular and plate-like martensite particles. Very fine martensite particles are distinguishable in the micrographs. These particles are frequently observable on the grain boundaries of ferrite. Their size
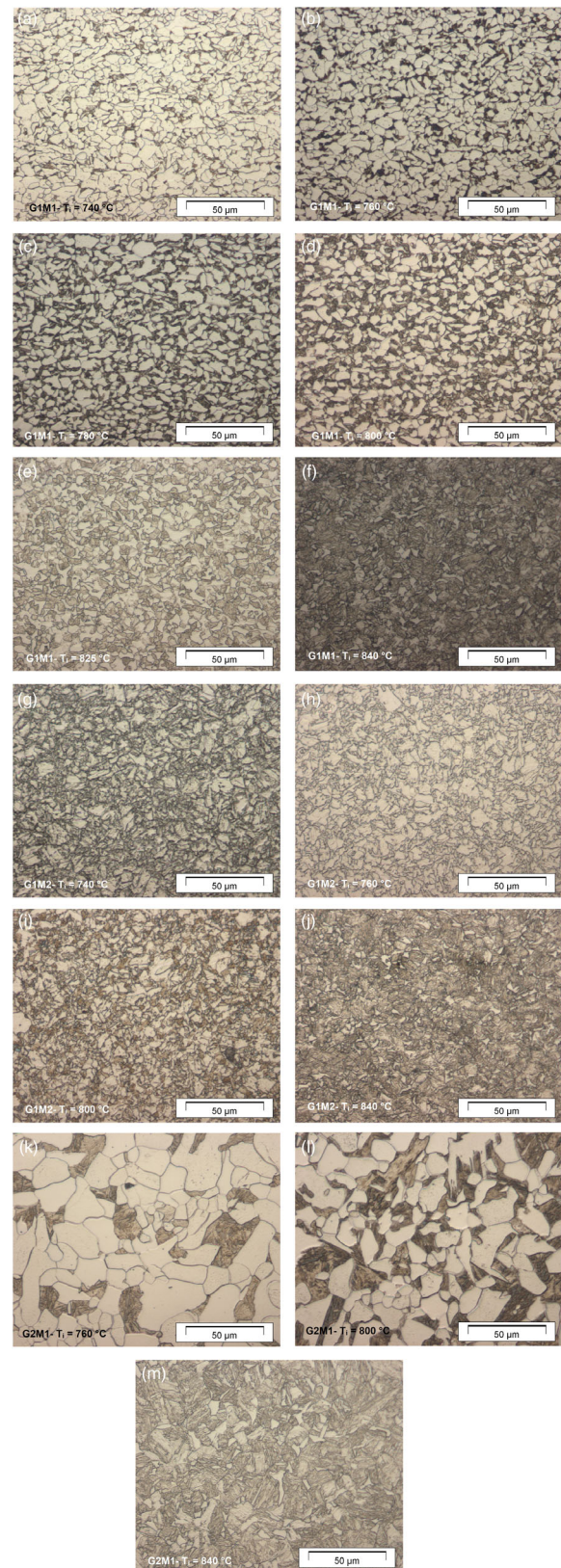

Figure 2. LOM micrographs of the three conditioned material groups: G1M1, G1M2, and G2M1.

**ADVANCED
SCIENCE NEWS**

www.advancedsciencenews.com

**steel
research**
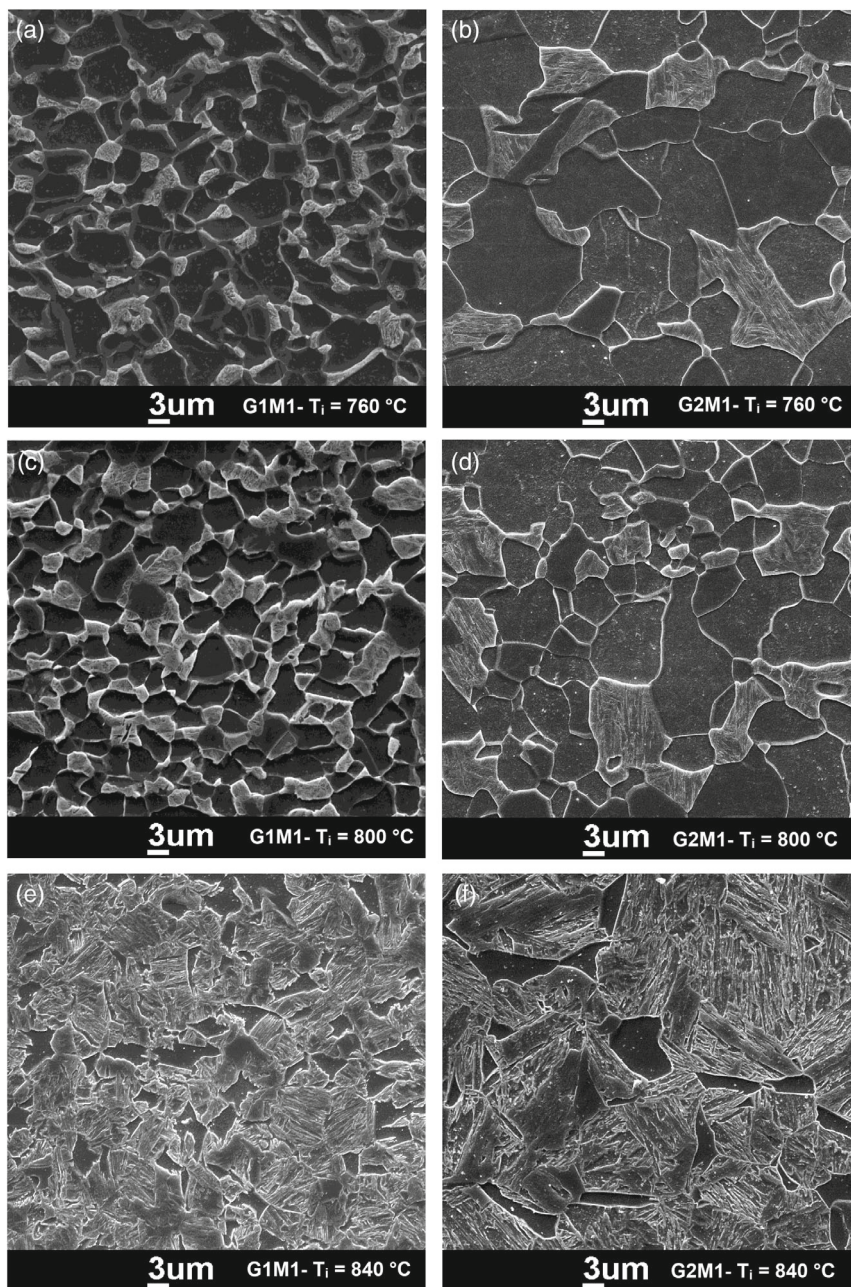international

www.steel-research.de

Figure 3. Representative SEM micrographs of G1M1-microstructures (left) and G2M1-microstructures (right).

increases with increasing the annealing temperature, whereas their number decreases.

The microstructure morphology and dispersion in the three conditioned material groups depend on the process of austenite formation and decomposition. During the direct intercritical annealing from the DP microstructure to produce the G1M1 microstructures, the austenite nucleates at and formed from the tempered martensite phase. Increasing the intercritical annealing temperature results in a growth of the formed austenite grains at the expense on the ferrite ones. In the case of intermediate quenching before intercritical annealing to produce the G1M2 microstructures, reheating the martensite in the ferrite–austenite phase region results in nucleation of austenite along the lath boundaries of the prior martensite. This results in a distribution of a fine elongated form of martensite and ferrite. In G2M1 microstructures, reheating to $1000\,°C$ results in the formation and growth of austenite grains. By subsequent intercritical annealing, the ferrite nucleates at the prior austenite grain boundaries. The coarse structure obtained in these microstructures is due to the coarse size of their prior austenite grains.

In all conditioned materials, decreasing T_i results in rising the ferrite quantity and increasing its grain size, whereas V_m
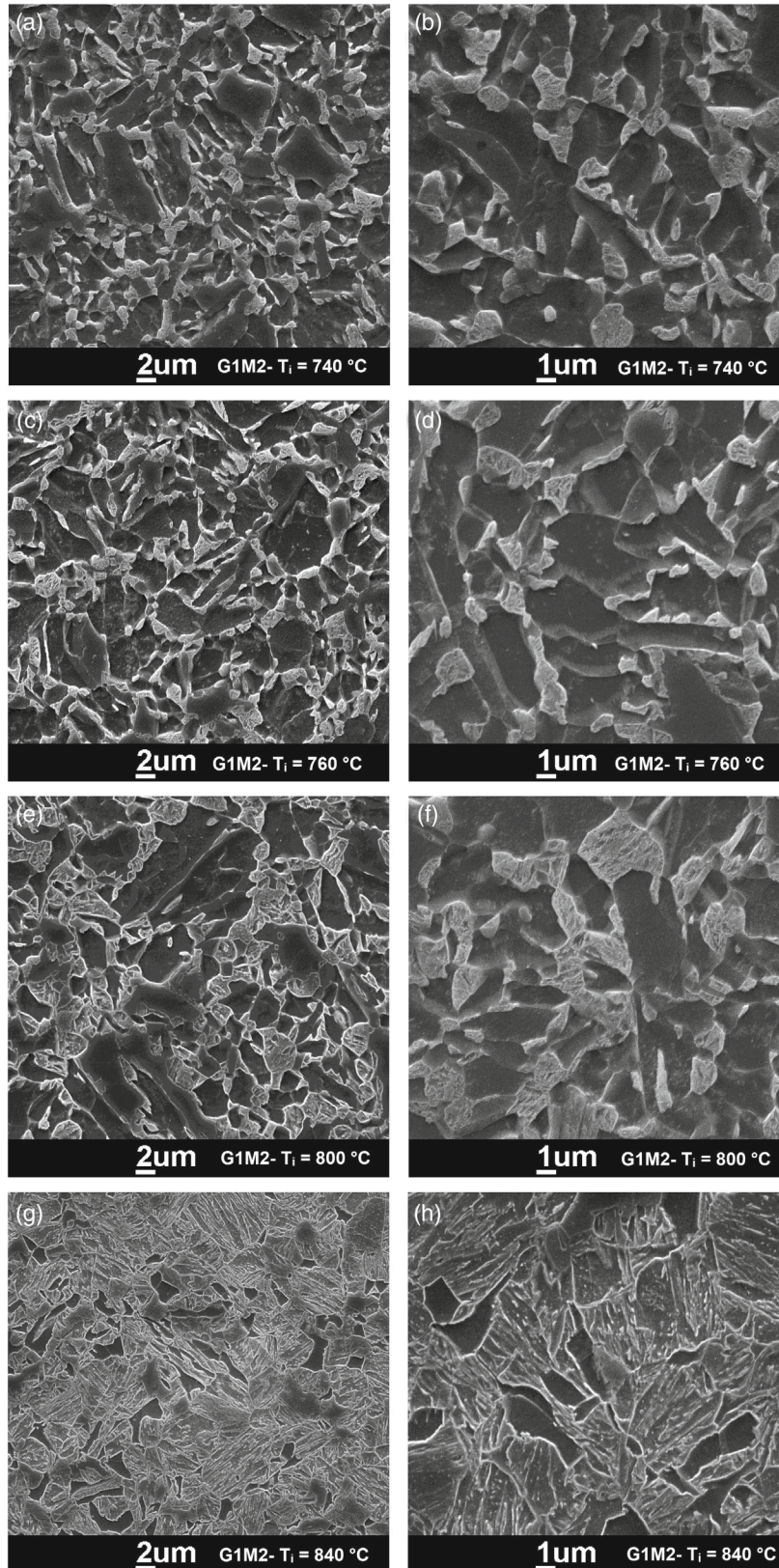
2000518 (4 of 15)

**ADVANCED
SCIENCE NEWS**

www.advancedsciencenews.com

**steel
research**
international

www.steel-research.de

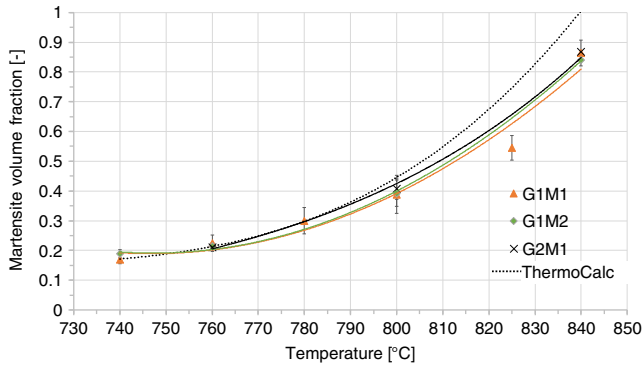**Figure 4.** SEM micrographs of G1M2-microstructures.

Figure 5. Comparison of dependence of austenite volume fraction predicted by ThermoCalc and that measured in the three conditioned DP steels.

decreases. **Figure 5** compares the calculated V_m obtained from ThermoCalc calculations with that measured for the different heat treatment cycles used. One can see that, instead of different starting microstructures before the intercritical annealing, the annealing proceeds to similar final amount of the intercritical austenite, which transforms via quenching to martensite. Accordingly, by the mass–balance relationship among the phases under equilibrium, V_m in the final microstructure should remain unaffected by the structure fineness and morphology with the unique factor affecting this balance being the T_i. The prior structure fineness and morphology would particularly affect the rate of transformation as previously illustrated by Soliman and Palkowski.[31] This observation indicates that 20 min of holding at T_i was sufficient for achieving the equilibrium state in all cases. Indeed, microstructural investigations illustrate that increasing the holding times in the intercritical region beyond the 20 min show an insignificant effect on the developed V_m.

On the other hand, the measured V_m values for T_i up to 800 °C have similar values as the predicted ones using the ThermoCalc software. The measured values of V_m above 800 °C are significantly lower than the predicted one.

Concurrent to the increase in V_m by increasing T_i, the martensite particle size d_m increases, while the ferrite grain size d_f decreases, as shown in **Figure 6**a,b. This behavior is basically correlated to the mechanism of nucleation and growth of austenite in G1M1 and G2M1microstructures and of ferrite in G1M2 microstructures; it indicates that the V_m increase by increasing T_i occurs basically via the increase in the size of the already nucleated phase in the former case and its decreases in the latter one; and not via new nucleation.

The dependence of the mean free path in ferrite, λ_f on V_m is shown in Figure 6c. This dependence is fitted by a logarithmic function. The extrapolated curves (dash line) should meet at the point $\lambda_f = 0$ at $V_m = 1$. Indeed, this point is an inevitable of the λ_f–V_m dependence; that is irrespective of the microstructure characteristics, a fully martensitic matrix ($V_m = 1$) implies that $\lambda_f = 0$.

3.2. Tensile Properties

Figure 7 shows representative engineering stress–strain curves for the different heat treatment conditions. The curves show
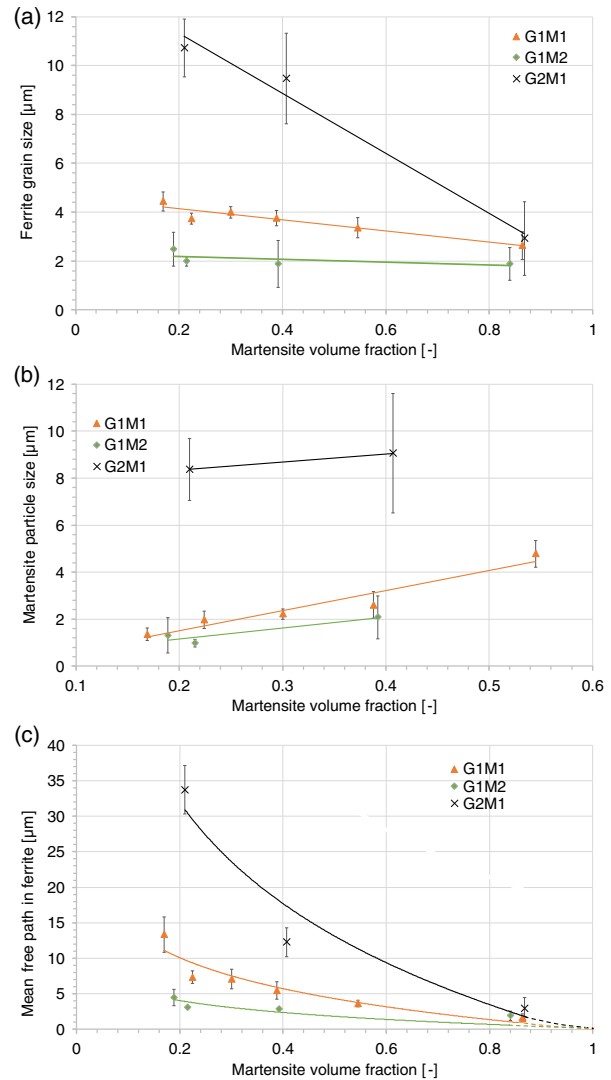

Figure 6. Dependence of the microstructure parameters: a) ferrite grain size, b) martensite grain size, and c) mean free path in ferrite on the martensite volume fraction.

typical characteristics of the tensile behavior of DP steels with low yield strength, continuous yielding, and high strain hardening. The curves of Figure 7c indicate that refining the grain size of the DP steels with the globular morphology (M1) strongly enhanced its strength without scarifying ductility.

The influence of V_m on the strength and ductility of the studied DP steels is shown in **Figure 8**. Increasing V_m results in a strength increasing at the expense of the ductility. The ultimate tensile strength (R_m) and the 0.2% proof strength ($R_{p0.2}$) dependencies on V_m can be fitted with a linear function, see Figure 8a. The linear relationship between strength and V_m was also stated by other researchers.[3,32,13,16] The G1M2 microstructures showed the highest strength which is correlated to its very fine structure. In addition, Sun and Pugh concluded that tensile strengths and elongations of DP steels depend not only on the martensite volume fraction but also on the morphology of
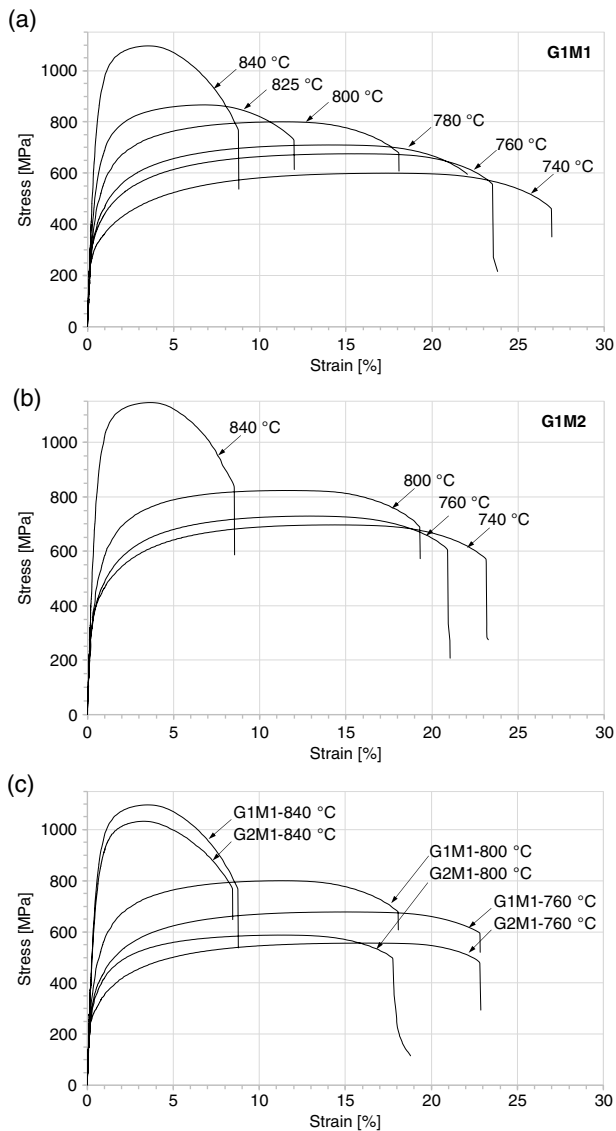
**ADVANCED
SCIENCE NEWS**

www.advancedsciencenews.com

**steel
research**
international

www.steel-research.de

(a)

(b)

(c)

Figure 7. Representative engineering stress–strain curves of a) G1M1 structure, b) G1M2 structure, and c) comparing the curves of G2M1 with G1M1 structure.

the second phase; DP steels with elongated structure "fiber" show higher but lower ductility.[19]

Figure 8 also points out that the coarse structures in G2M1 resulted in significantly lower strengths. Interestingly, however, is that the uniform elongation of these coarser structures is almost similar with that obtained for G1M1. The observation that the conventional tradeoff between strength and ductility does not apply when refining the microstructure of DP steels is in consistence with previous studies: Calcagnotto et al.[24] reposted that ε_u and ε_t are only slightly affected by decreasing d_f from 12.4 to 1.2 μm. It is also shown in the work of Delincé et al. that a decrease in ductility becomes significant only when the ferrite grain size of the DP steel is reduced below ≈2 μm.[33] This insignificant effect of decreasing d_f on ε_u can be attributed to an increase in strain hardening with decreasing grain size.[14,33]
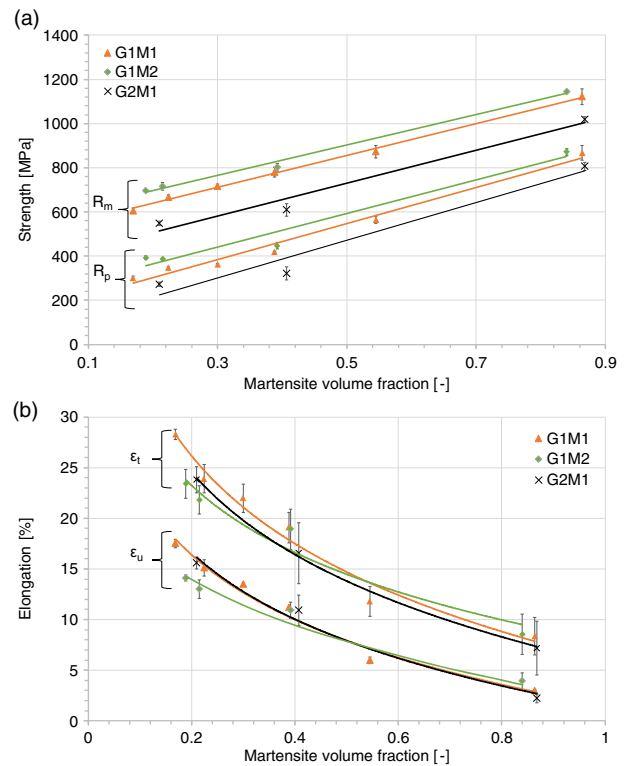
(a)

(b)

Figure 8. Dependence of the a) yield- and tensile strength and b) uniform- and total elongation on the martensite volume fraction.

The dependence of strain hardening on d_f of the studied steels will be shown under Section 3.5.

Even so, Figure 8b shows that the mean value of ε_t for G2M1 structures showed inferior values compared with G1M1 structures. Indeed, the values of ε_t are strongly affected by the geometric instability occurring in the samples after necking during tensile testing, which in turn reduces the reproducibility of ε_t values.[13] The low reproducibility of ε_t is revealed by the relatively large error bars. The observed inferior ε_t of G2M1 may indicate that coarsening the structure promotes the geometrical instability after necking. Similarly, it was previously observed that the tensile samples of DP steels with finer grain size exhibits more pronounced necking the postuniform elongation increases with decreasing grain size.[14]

The G1M2 steel annealed at 740 °C ($V_m = 0.18$) and that annealed at 760 °C ($V_m = 0.22$) show significant inferior ductility, as shown in Figure 8b. These structures show a substantially elongated character, see Figure 4a–d. The plastic constraint imposed by this martensite form is significantly higher than that imposed by the more spherical-shaped martensite. Therefore, at a constant martensite volume fraction, the structure with more spherical-shaped martensite shows better ductility. The structures annealed at 800 and 840 °C shown in Figure 4e–f are not as strongly elongated as that ones annealed at 740 and 760 °C. Similarly, Zhang et al. observed that fibrous martensite gradually transformed to blocky martensite with an increase in intercritical annealing temperature. This can justify the observation that the ductility of the steels annealed at 800 and 840 °C is
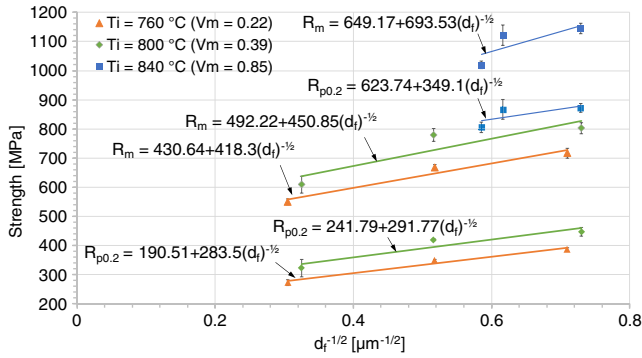
Figure 9. Effect of grain size on the strength of the DP steels.

only slightly affected by the microstructure morphology, as shown in Figure 8b.[20]

The enhancement of both yield strength and tensile strength due to grain refinement is shown in **Figure 9**. The yield and tensile strength both follow the linear Hall–Petch relationship between strength and inverse square root of ferrite grain size by the equation:

$$\sigma = \sigma_0 + c(d_f)^{-1/2} \qquad (2)$$

where σ_0 and c are constants.

The applicability of the Hall–Petch relation between yield strength and ferrite grain size in DP 259 steels was also shown by Jiang et al.[26] and Calcagnotto et al.[24] It can be inferred from Figure 9 that R_m is more strongly affected by the ferrite grain refinement than $R_{p0.2}$ as can be deduced from the higher c values of R_m when considering the same V_m. In addition, a gradually rising in the rate of increasing the strength due to the grain refinement (c value) with increasing V_m in both cases of $R_{p0.2}$ and R_m is observed. This observation is opposite to that shown by Peng-Heng and Preban, who observed a stronger effect of structure refinement on yield strength than on the tensile strength.[22]

3.3. Strain Hardening Behavior

The high strain hardening is an important advantage of DP steels compared with other advanced high strength steels. The DP steels exhibit low yield strength, which facilitates cold forming but its high strain hardening rate determines the possibility of a significant increase in strength after deformation. The strain hardening is therefore an indicator of their stretchability during press forming operations. On the physical level, strain hardening is due to an increase in dislocation density during forming. The plastic incompatibility between ferrite and martensite leads to the formation of back stresses in the ferrite phase. These back stresses restrict dislocation movement in the ferrite phase.[34] The high strain hardening value of the DP steels enables its deformability before instability, and the material can be stretched further before necking starts, thus enabling a component to be formed with less localized thinning.[1,35]

The most common parameter of strain hardening is the exponent n in the parabolic approximation of stress–strain σ–ε curve introduced by Hollomon[36]

$$\sigma = k \cdot \varepsilon^n \qquad (3)$$

where σ and ε are the true stress and true strain, respectively.

The coefficients n can be obtained by plotting the true stress–true strain curve on a logarithmic scale

$$\ln \sigma = \ln k + n \ln \varepsilon \qquad (4)$$

Figure 10 shows the variation of $\ln \sigma$ with $\ln \varepsilon$ for the investigated DP steels. A criterion for the linear fitting of $\ln(\varepsilon)$–$\ln(\sigma)$ is adopted, in which the number of fitting lines are kept to a minimum considering that the least square regression factor (R^2) value of these lines stay above 0.995. Dividing the flow curve of DP steel to different n values is necessity because defining
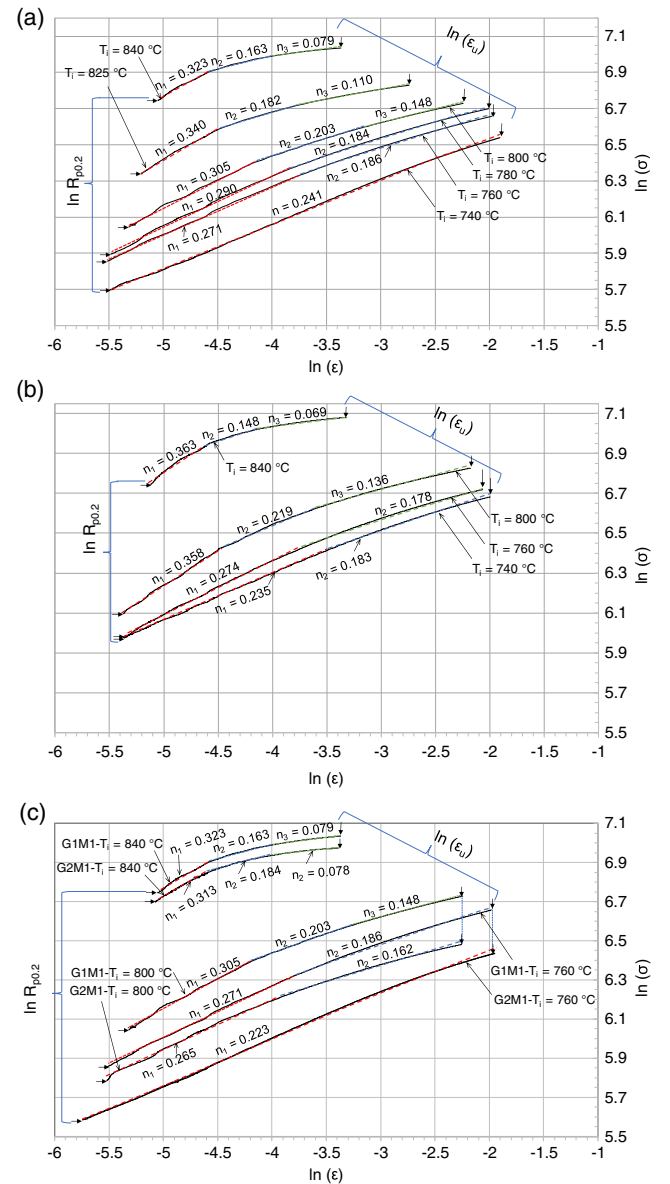

Figure 10. $\ln \sigma$ versus $\ln \varepsilon$ plots for the Hollomon analysis of the strain hardening behavior of: a) G1M1, b) G1M2, and c) comoaring G2M1 with G1M1; the slopes of line segments are equivalent to n-values.

the different n values and the range of strain that they cover are of great importance for designing the cold forming operation (indication of the stretchability). In particular, identifying the remarkably large work hardening that occurs at small plastic strains (n_1) is crucial for designing the forming process. This value largely differs from the recorded one before necking (n_3), as shown in Figure 10. The latter value covers a strain range that the steel typically not stretched to.

As shown in Figure 10, up to three stages of strain hardening can be identified. Indeed, many authors identified two hardening stages of DP steels,[26,37–41] others showed three stages of strain hardening.[10,15,42–44] Figure 10 shows that the DP steels can also exhibit a single stage strain hardening. A linear behavior is observed for the G1M1 steel annealed at 740 °C, i.e., the one with the lowest martensite content. G2M1 exhibits this linear behavior for samples annealed at 760 °C. With increasing the V_m, the samples exhibit nonlinear variations of ln σ with ln ε and two to three strain hardening stages are perceived in both cases of G1M1 and G2M1. Regarding the G1M2, the steel exhibited two to three stages of strain aging for all studied V_m. It is important to mention here that the change in the strain hardening immediately before reaching ε_u is not considered as an additional changing in the hardening behavior.

Table 1 shows a list of the estimated n values for the different DP steels produced. The strain hardening is the highest at the beginning of plastic deformation. This is interpreted as a result of an initial high density of free dislocations and hence higher rates of dislocation accumulation and multiplication within this strain range.[2,26,44] The second stage (stage 2) with the lower slope is related to restraining the ferrite deformation by the martensite.[44] The material with the lowest V_m of about 0.17 ($T_i = 740$ °C) in G1M1 microstructure, did not show a second stage. For this case, constraining the ferrite deformation with a low amount of martensite is limited and therefore a second strain hardening stage does not occur. At higher martensite contents, a third stage (stage 3) with the lowest work hardening ability is observed. The appearance of this stage indicates the codeformation of both the ferrite and martensite.[44]

Jiang et al. suggested that within a certain strain interval, the deformation state of martensite changes from elastic to plastic.[26] The absence of this stage in the material with lower martensite content indicates that the martensite phase is not deformable under this condition. Indeed, increasing the martensite content of DP steels results in dilution of alloying elements in the intercritical austenite, which transforms during quenching to martensite. For instance, thermodynamic calculations using ThermoCalc showed that at $T_i = 760$ °C, the C concentration in austenite has a value of 0.29 wt%. This concentration decreased to 0.15 wt% when increasing the T_i to 800 °C.[13] Delincé et al. reported that with increasing V_m, the martensite becomes softer and starts deforming plastically.[33] Jiang et al. analyzed the strain hardening plots to estimate the quantity of V_m at which the martensite phase in DP steels starts to deform plastically.[26] The onset of plastic deformation of martensite in DP steel was predicted to depend on its yield strength and the microstructural variables.

In the framework of this study, two alloys with the chemical composition of the intercritical austenite and intercritical ferrite at $T_i = 760$ °C to correspond to the two phases of the DP annealed at this temperature have been cast. The alloy with the composition of the intercritical austenite was annealed and quenched to obtain a fully martensitic structure, whereas that with the ferrite composition was normalized by heating to 920 °C and cooling in air. The microstructures of the two alloys after the heat treatments are shown in **Figure 11**. The obtained grain size of the ferritic alloy is similar to that of the G2M1 microstructure (Figure 2g). The tensile curves of the two alloys are shown in **Figure 12**a. As shown in this figure, the martensitic samples did not show any deformability but fractures before reaching the yield point. This supports the hypothesis that the martensite does not participate in the deformation of the DP annealed at 760 °C and therefore the third strain hardening stage, which appears due to martensite deformation, is absent for this case. It is important to mention here that the martensitic samples were not subjected to a tempering treatment, this is to be equivalent to the nontempered martensite of the DP steel.

Figure 12a also shows the stress–strain curve of the ferritic phase. This curve is characterized by discontinuous yielding and a high strain hardening capacity. Figure 12b shows that the single-phase ferrite alloy shows a single strain hardening stage with an n value significantly higher than that of both the G1M1 and G2M1 material annealed at 760 °C (G2M1 have similar d_f as that of the single phase ferrite alloy). This observation supports the presumption that the multistage strain hardening and the decrease of the n value in the subsequent strain hardening stages is related to the presence of martensite as a second phase.

In summary, the number of strain hardening stages in DP steels can diminish from three to two stages at lower V_m. This is because of the nondeformable intrinsic characteristic of martensite, when its quantity goes below a certain level. By a further decrease in V_m, here 0.17 for G1M1 and 0.21 for G2M1, the constraining effect of martensite for ferrite deformation becomes insignificant and hence only one strain hardening stage can be observed. The previous analysis may explain the controversy regarding the number of strain aging stages of DP steels reported in the literature. This number is proposed here to be
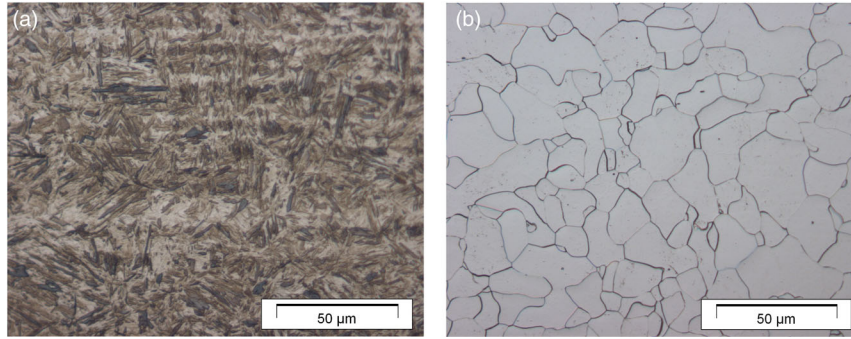
Table 1. List of the n values estimated for the prescribed heat treatment conditions.

	T_i [°C]	V_m	$n1$	$n2$	$n3$
G1M1	740	0.169	0.241	–	–
	760	0.224	0.271	0.1860	–
	780	0.300	0.290	0.1840	–
	800	0.388	0.305	0.203	0.148
	825	0.545	0.340	0.182	0.110
	840	0.864	0.323	0.163	0.079
G1M2	740	0.189	0.235	0.183	–
	760	0.215	0.274	0.178	–
	800	0.392	0.358	0.219	0.136
	840	0.84	0.363	0.148	0.069
G2M1	760	0.21	0.2234	–	–
	800	0.407	0.265	0.162	–
	840	0.868	0.313	0.184	0.078

**ADVANCED
SCIENCE NEWS**

www.advancedsciencenews.com

**steel
research**
international

www.steel-research.de

Figure 11. LOM micrographs of the two produced steels with compositions corresponding to the ones of a) martensite and b) ferrite of the DP steels, intercritically annealed at 760 °C.
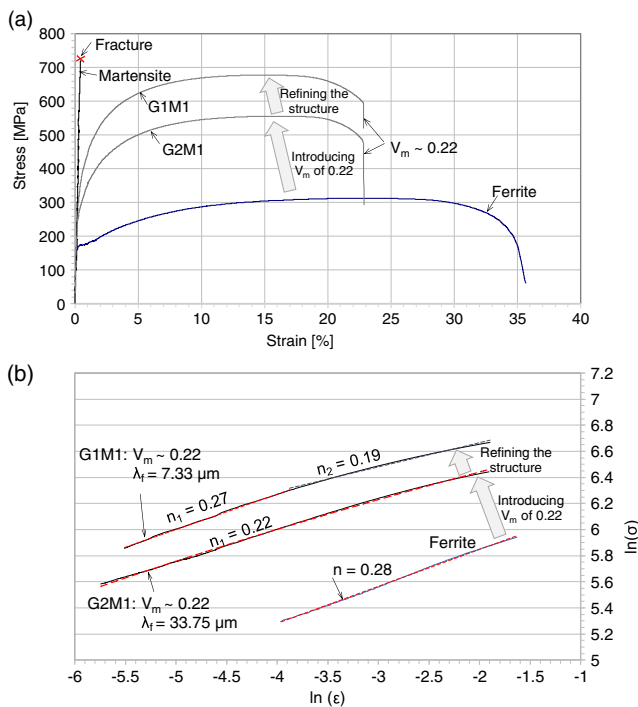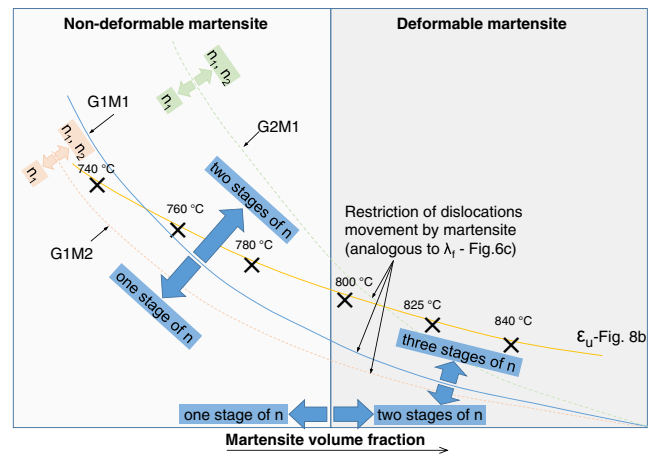

Figure 13. Schematic illustration of the way in which the DP steels' parameters can interact, to yield one, two, or three stages strain hardening. Please note that changing the conditioned material group results in moving the boarder-curve G1M1 to the dashed curves G2M1 or G1M2 (Figure 6c). Changing the structure to G2M1 or G1M2 can eventually also affect ϵ_u (Figure 8b) and the line separating the deformable and nondeformable martensite. ×: represents the necking point at the prescribed temperatures.

Figure 12. a) stress–strain curves and b) ln σ versus ln ε plots of the single-phase steels and the DP steels annealed at 760 °C with G1M1 and G2M1 structures.

correlated to the martensite content and its deformability. **Figure 13** shows schematically the way in which the materials' parameters can interact, based on the previous discussions, to yield one, two, or three stages of strain hardening. In this diagram, the curves representing the dependence of the restriction of dislocations movement by martensite phase on V_m are represented by curves with trends similar to the dependence of λ_f on V_m (Figure 6c).

The schematic diagram of Figure 13 shows the reason for observing a lower number of strain hardening stages in the G2M1 microstructure annealed at $T_i = 760$ and 800 °C than observed in the G1M1 microstructure (Table 1). The larger mean free path in ferrite, λ_f of G2M1 microstructures (the green

dashed curve is shifted to higher values) gives more space for the multiplication of dislocation. Accordingly, stage 2, in which this multiplication is restrained by martensite grains, is obscure. The necking for the material annealed at $T_i = 760$ °C and the martensite deformation for that annealed at $T_i = 800$ °C took place earlier and therefore, only one strain hardening stage appears in the former and two stages in the latter, as shown in Table 1 and Figure 13. Similarly, the reason that the G1M2 microstructure demonstrated two stages of strain hardening at 740 °C, though exhibiting a low V_m, can be attributed to its lower λ_f value, so the dislocation multiplication is constrained by martensite earlier; i.e., before necking.

The schematic diagram of Figure 13 shows a base for developing a model that defines the number of strain hardening stages occurring in DP steels. So far, this model is not available in the literature. Defining the border separating the deformable martensite from the nondeformable one, by, e.g., applying the methodology suggested by Shen et al.,[45] is essential for a reliable

definition of the model. This diagram together with the available results present a basis that can be utilized for developing and calibrating a micromechanical model that considers the alteration of the strain hardening behavior of DP steel with varying the straining value.

As shown in Figure 10, it can be observed that there is no distinct point of changing from one stage to the other, but the change took place progressively. This can be attributed to the relative inhomogeneities in martensite distribution and the heterogeneous deformation of the ferrite matrix. Therefore, the dislocations cannot be assumed to be obstructed by the martensite particles at the same time and that the martensite particles cannot be assumed to deform plastically simultaneously. Accordingly, the alternation among the different stages of the strain hardening capacity takes place gradually.

3.4. C-J and Modified C-J Analysis

In the framework of this study, it was important to confirm the number of work hardening stages and the strain range of its each stage applying other analytical methods. In this section, the applicability of two other equations, rather than the Hollomon equation, and the corresponding analyses to the presentation of the strain hardening behavior of the studied DP steel is examined. The two equations are:

Ludwik equation[46]

$$\sigma = \sigma_0 + k_L \cdot \varepsilon^{nL} \tag{5}$$

and

Swift equation[47]

$$\sigma = A(B + \varepsilon)^{ns} \tag{6}$$

The Swift equation can be written as

$$\varepsilon = -B + k_S \sigma^m \tag{7}$$

where $k_S = A^{-\frac{1}{n_s}}$ and $m = \frac{1}{n_s}$.

Equation (5)–(7) is extensions of the Hollomon model with additional parameters. σ_0 is the stress at the yielding point of steel. n_L and n_S are strain hardening exponents, and k_L and k_S are material constants. The B factor is the prestrain coefficient, explicitly the prestrain $(\varepsilon_P) = -B$ when substituting $\sigma = 0$ in Equation (7), therefore, the value of B presents the intercept of the Swift curve with the true-strain axis. The B value cannot take negative value because the extension of the flow curve should intersect the abscissa at negative ε_P. The Swift equation is reduced to the Hollomon equation, if $B = 0$, i.e., by neglecting the prestrain coefficient.

The Crussard–Jaoul (C–J) analyses[48,49] of strain hardening is based on Ludwig equation, whereas the modified C–J analyses[50] is based on Swift equation. By differentiating Equation (5) and (7) and expressing them in logarithmic forms:

C–J analysis

$$\ln(d\sigma/d\varepsilon) = (n_L - 1)\ln\varepsilon + \ln(k_L n_L) \tag{8}$$

and modified C–J analysis

$$\ln(d\sigma/d\varepsilon) = (1 - m)\ln\sigma + \ln(k_S m) \tag{9}$$

Representative plots of the ln $(d\sigma/d\varepsilon)$ against ln ε (C–J analysis) and ln $(d\sigma/d\varepsilon)$ against ln σ (modified C–J analysis) are shown in **Figure 14**. It is obvious in this figure that the C–J analysis seemingly shows that the studied steels have a single strain hardening coefficient, n in the G1M1 microstructures annealed at 780, 800, and 840 °C (Figure 14a,c,e), whereas those annealed at 740 °C showed two stages of strain hardening (Figure 14a). These observations are contradicting to those perceived applying the Hollomon analysis (Figure 10).

Similar to the current results, Colla et al. have not marked any slope change in the C–J plots in their DP steels studied.[41] An earlier report of Tomita and Okabayashi showed that the C–J analysis is less sensitive to changes of the ferrite matrix and the shape and distribution of the second phase martensite, which were altered by the heat treatments.[37] Likewise, the C–J method is also not appropriate for describing work hardening of the DP steels investigated in this study.

Nevertheless, several authors studied the work hardening of DP steels applying C–J analysis and reported up to three strain hardening stages applying this method.[15,16,51] It is worth mentioning here that the obtaining inversed slope, indicated by an arrow in Figure 14c, is an artifact that cannot be interpreted as a change in strain hardening capacity. The points of slope change in this figure do not coincide with the corresponding ones in Figure 10a. A similar inversed slope is also observed by Bag et al., who interpreted it as three-stage work hardening behavior.[15] This interpretation is actually not in consistence with the normal behavior of the n factor which cannot have an intermediate inversed alteration. According to Jiang et al.[26] and Colla et al.,[41] the C–J analysis presents linear regions in the ln $(d\sigma/d\varepsilon)$ versus ln ε curves, with slopes in the first (low-strain) stage larger than those in the second (high-strain) one.

Figure 14b,d,f,g,h shows representative modified C–J plots of the DP steels. All plots—except that one of G1M1 microstructures annealed at $T_i = 740$ °C—deviate from linearity over the uniform strain range; a single n value could not be assigned to the entire curve. These curves can be fitted by two or three fitting lines. For instance, two lines are required for fitting the plots of G1M1 annealed at $T_i = 780$ °C, G1M2 annealed at 740 °C and G2M1 annealed at 800 °C (Figure 14b,g,h, respectively), whereas three lines are required for fitting the plots of G1M1 with $T_i = 800$ and 840 °C, Figure 14d,f. These observations are consistent with the Hollomon analysis, as shown earlier (Figure 10). Considering the same conditioned microstructure, both analyses show the same number of strain hardening stages with similar estimated points of the changing in their values.

Considering to the C–J and modified C–J methods in this study has enabled assessing the suitability of both methods for defining the strain hardening behavior of DP steel and used for verifying the number of strain hardening stages. Nevertheless, assessing the n values relied only on the Hollomon method.

3.5. Factors Affecting Strain Hardening Values

Referring to Table 1, it can be inferred that increasing V_m results not only in increasing the number of the strain hardening stages
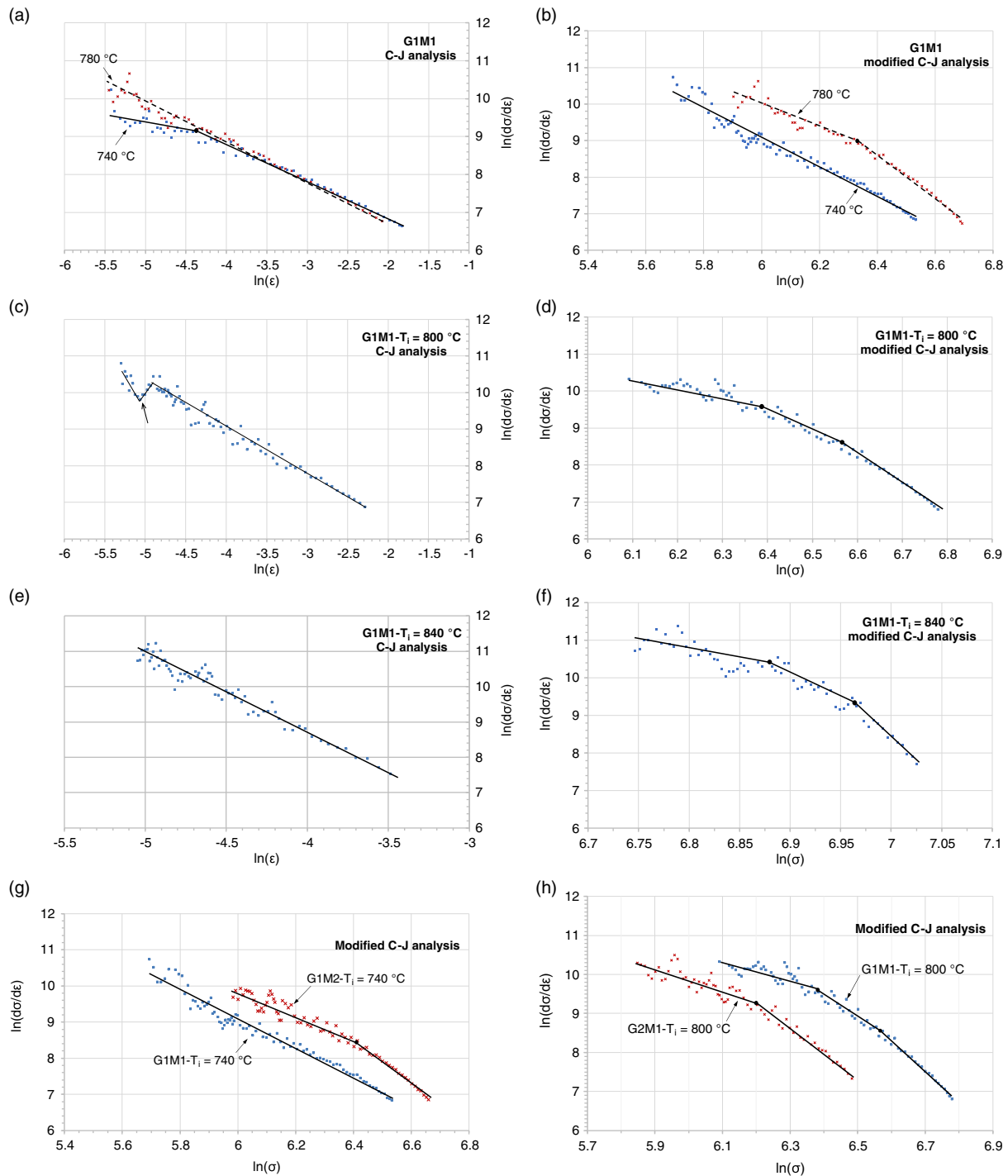
Figure 14. a,c,e) representative plots of ln (dσ/dε) against ln ε (C–J analysis) and b,d,f,g,h) representative plots of ln (dσ/dε) against ln σ (modified C–J analysis). The treatment conditions are prescribed on the plots.

but also in increasing the strain hardening capacity in the first stage (n_1). The higher V_m results in inducing more dislocations in the ferrite which are formed during martensitic transformation from the austenite, i.e., during quenching. The increased V_m can be attributed to a higher dislocation density in ferrite, which results in higher rates of dislocation accumulation and

multiplication occurring during straining and hence in a higher n value.[10,44] The total number of generated dislocations is also dependent on the ferrite quantity, the volume fraction of ferrite for the DP quenched from $T_i = 840\,°C$ is so low that their number decreases and consequently the n_1 factor can accordingly decrease as the case of the G1M1 structure.

On the other hand, considering similar V_m, the G1M2 shows slight increases in n_1 values compared with the G1M1 structure, whereas the G2M1 structure shows a significant decrease in its n_1 value. Indeed, the martensite ferrite interface increases by both of refining the structure and changing its form to a lamellar one, accordingly the induced geometrically necessary dislocations (GNDs) increase and develop more homogeneous, therefore the material shows higher work hardening capacity. Similarly, Kundu and Field reported that work hardening in small grain DP steels is higher than that in ones with the large grains.[52]

In summary, increasing V_m, refining the structure and changing its morphology to an elongated one results in increasing the number of strain hardening stages and improving the strain hardening capacity in the first stage (n_1).

Indeed, the most striking property of DP steels is the remarkably large work hardening which occurs at small plastic strains, i.e., n_1.[8] A simplifying assumption that can be made is that the mean free path in ferrite, λ_f could be the single most significant factor of all the independent variables, influencing the n_1 factor. The obtained value of n_1 is closely related to the plastic flow in the first ferrite to deform, which starts with the lowest dislocation density and spreads through the ferrite with increasing densities of dislocations as the applied stress is increased. Correlating n_1 to λ_f is based on the hypothesis that the prescribed development and evolution of the dislocations in ferrite is strongly affected by λ_f. The dependence of n_1 value on λ_f is shown in **Figure 15**. It is interesting that a single curve is well fitting the data points of both of G1M1 and G2M1 concurrently, including that of G2M1 at very high λ_f value of $\approx 34\,\mu m$. Accordingly, for a globular structure, λ_f can present a generalized factor affecting n_1 that not only incorporates the V_m but also the d_f factor. For comparison, relating the n_1 factor to λ_f is shown to be dependent of the microstructure morphology, i.e., an additional fitting curve is required for fitting the G2M1 microstructure, as shown in Figure 15. The n_1 value of the morphology M2 shows a stronger dependence on λ_f than that of the M1 morphology. Moreover, the DP steels with M2 morphology exhibit higher strain hardening compared with those ones with the morphology M1, up to a threshold λ_f.

3.6. Strain Hardening after Aging

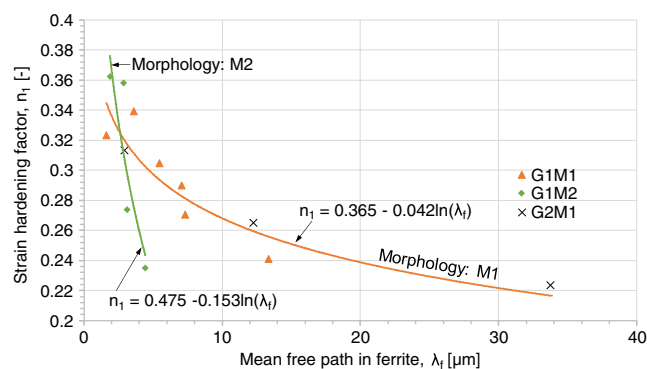To investigate the effect of aging on the strain hardening capacity of DP steels, selected conditioned DP steels were aged at 170 °C for 20 min. The tensile curves after aging are shown in **Figure 16**a. A table comparing the tensile properties before and after aging is integrated in Figure 16a. As can be inferred from this table and when comparing Figure 16a with Figure 7, the aging treatment results in a strong increase in yield strength accompanied by an occurrence of discontinuous yielding phenomena. This yield strength increase is attributed to dislocation locking due to the formation of Cottrell atmospheres around dislocations and grain boundaries or precipitation of transition carbides in ferrite. The pinning leads to the occurrence of a more distinct yield point, as new mobile dislocations must be created to initiate plastic flow. Furthermore, aging the DP steels resulted in a significant decrease in the tensile strength accompanied by a slight enhancement of the total elongation as shown in the table inserted in Figure 16a. A similar result is reported by other authors in previous works.[24,53,54] In the work of Ramazani et al. only the non-pre-strained samples showed the ductility increase and the decrease in strength.[54] Indeed, the diffusion of carbon from the super saturated ferrite to the dislocations, causing the yield strength increase, results also in decreasing the free carbon, saturating the ferrite phase, accordingly a softer ferrite results from the aging process. The reduction in the amount of carbon supersaturating the ferrite due to aging was experimentally confirmed by Nakaoka et al.[55] The aging process may also result in a tempering effect in the martensite, which would also enhance the elongation and reduce the tensile strength.
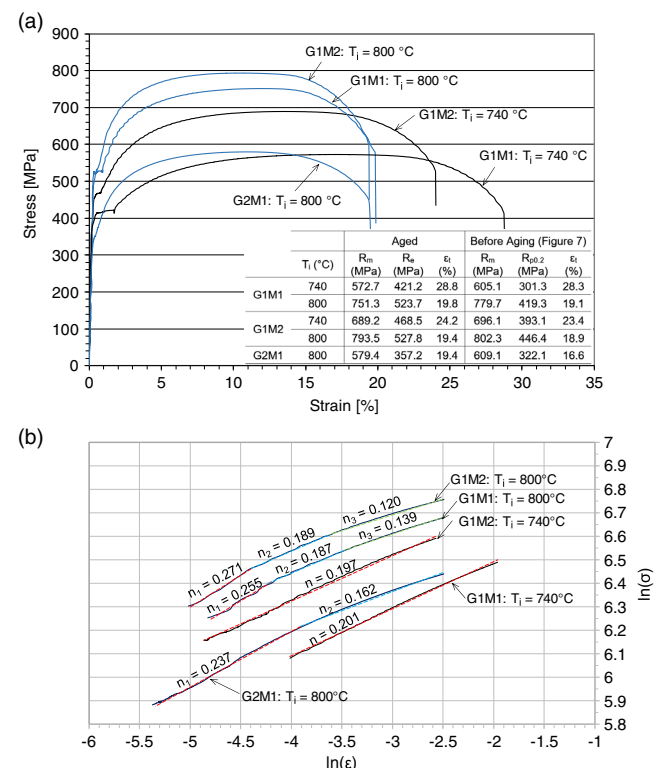

Figure 15. Dependence of strain hardening factor n_1 on the mean free path in ferrite.

Figure 16. a) Stress–strain curves of DP steels after aging together with a table listing the tensile properties before and after aging b) $\ln \sigma$ versus $\ln \varepsilon$ plots of the aged DP steels given in (a).

By comparing the strain hardening values shown in Figure 16b with the corresponding ones shown in Table 1, it can be concluded that the aging process results in a significant decrease in the strain hardening capacity of the DP steels in all cases. The combined effects of the increase in yield strength and decrease in tensile strength caused the lower strain hardening capacity of the aged DP steel.

4. Conclusions

This investigation presents an extensive study on the microstructure-tensile properties relationship in DP steels. A series of ferrite and martensite DP steels with different martensite volume fractions (V_m), different morphologies, and different grain sizes were produced by applying appropriate heat treatments. From the results of this study, the following conclusions can be drawn: 1) The V_m in the final microstructure remains unaffected by the structure fineness and morphology with the unique factor affecting it being the intercritical annealing temperature, T_i. This observation indicates that the 20 min of holding at T_i was sufficient for achieving the equilibrium state in all cases. 2) Decreasing T_i results in increasing the quantity of the ferrite phase and increasing its grain size, whereas the martensite fraction and its particle size decreases. 3) Refining the microstructures of DP steels with globular morphology (M1) strongly enhanced its strength without compromising the ductility. At low T_i, DP steels with elongated structure (M2) show increased strength but lower ductility compared with the M1. The elongated structure gradually transformed to globular one with increasing T_i, accordingly the ductility at higher T_i is slightly affected by the microstructure morphology. 4) The strengthening of the studied DP steels due to the grain refinement is found to obey the Hall–Petch relation. A gradually rising in the rate of increasing the strength due to the grain refinement with increasing V_m in both cases of $R_{p0.2}$, and R_m is observed. The R_m is strongly affected by the ferrite grain refinement than the $R_{p0.2}$. 5) The plastic flow of the tensile curves revealed up to three stages of strain hardening with the highest strain hardening exponent at the beginning of straining. In this analysis, the work hardening behavior of the samples containing less than $V_m \leq 0.21$ is single stage. By increasing V_m, refining the structure and changing its morphology to M2, the number of strain hardening stages increased and the strain hardening capacity in the first stage (n_1) improved; noting that V_m represents the strongest affecting factor. The mechanism in which the DP steels' parameters can interact, to yield one, two, or three strain hardening stages is explored in this study. 6) The C–J analysis is less sensitive for strain hardening behavior of the studied DP steels and revealed misleading results. The analyses carried out by Hollomon and modified C–J methods showed good consistency. 7) The mean free path in ferrite, λ_f is the predominant factor affecting n_1 that incorporates the effects of both the V_m and d_f factors. Therefore, for the DP steels with similar morphologies, λ_f can represent a single microstructure factor affecting n_1 value. The n_1 value of the morphology M2 shows stronger dependence on λ_f than that of morphology M1. 8) The aging process results in improving yield strength and total elongation, however, the strain hardening capacity decreased significantly.

Conflict of Interest

The authors declare no conflict of interest.

[1] Y. Mazaheri, A. Kermanpur, A. Najafizadeh, *Mater. Sci. Eng. A* **2014**, *619*, 1.
[2] N. Fonstein, in *Automotive Steels, Design, Metallurgy, Processing and Applications* (Eds.: R. Rana, S. B. Singh), Woodhead Publishing – Elsevier Ltd., Duxford **2017**, pp. 169–216.
[3] R. G. Davies, *Metall. Trans. A* **1978**, *9*, 671.
[4] R. G. Davies, C. L. Magee, *Metall. Trans. A* **1978**, *9*, 41.
[5] N. K. Balliger, T. Gladman, *Met. Sci.* **1981**, *15*, 95.
[6] T. Gladman, *Met. Technol.* **1983**, *10*, 274.
[7] A. Sarosiek, W. Owen, *Scr. Metall.* **1983**, *17*, 227.
[8] A. M. Sarosiek, W. S. Owen, *Mater. Sci. Eng. A* **1984**, *66*, 34.
[9] Z. Zhao, X. Wang, G. Qiao, S. Zhang, B. Liao, F. Xiao, *Mater. Des.* **2019**, *180*, 1.
[10] Z. P. Xiong, A. G. Kostryzhev, N. E. Stanford, E. V. Pereloma, *Mater. Des.* **2015**, *88*, 537.
[11] M. Sarwar, E. Ahmad, K. A. Qureshi, T. Manzoor, *Mater. Des.* **2007**, *28*, 335.
[12] M. M. Karimi, S. Kheirandish, *Steel Res. Int.* **2009**, *80*, 160.
[13] M. Soliman, H. Palkowski, *Mater. Sci. Eng. A* **2020**, *777*, 139044.
[14] M. Calcagnotto, D. Ponge, D. Raabe, *Mater. Sci. Eng. A* **2010**, *527*, 7832.
[15] A. Bag, K. K. Ray, E. S. Dwarakadasa, *Metall. Mater. Trans. A* **1999**, *30*, 1193.
[16] T. S. Byun, I. S. Kim, *J. Mater. Sci.* **1993**, *28*, 2932.
[17] E. N. Birgani, M. Pouranvari, *Metal* **2009**, *19*, 1.
[18] M. Y. Sun, X. L. Wang, Z. Q. Wang, X. M. Wang, X. C. Li, L. Yan, R. D. K. Misra, *Mater. Sci. Eng. A* **2020**, *771*, 138668.
[19] S. Sun, M. Pugh, *Mater. Sci. Eng. A* **2002**, *335*, 308.
[20] J. Zhang, H. Di, Y. Deng, R. D. K. Misra, *Mater. Sci. Eng. A* **2015**, *627*, 230.
[21] N. J. Kim, A. H. Nakagawa, *Mater. Sci. Eng.* **1986**, *83*, 145.
[22] C. Peng-Heng, A. G. Preban, *Acta Metall.* **1985**, *33*, 897.
[23] M. Nouroozi, H. Mirzadeh, M. Zamani, *Mater. Sci. Eng., A* **2018**, *736*, 22.
[24] M. Calcagnotto, Y. Adachi, D. Ponge, D. Raabe, *Acta Mater.* **2011**, *59*, 658.
[25] S. Singh, T. Nanda, B. R. Kumar Singh, *Mater. Manuf. Process* **2016**, *31*, 2064.
[26] Z. Jiang, Z. Guan, J. Lian, *Mater. Sci. Eng., A* **1995**, *190*, 55.
[27] ASTM, *Standard Test Methods for Tension Testing of Metallic Materials*, ASTM E8 – 11, ASTM International, West Conshohocken, PA **2011**.

[28] ASTM, *Standard Test Method for Determining Volume Fraction by Systematic Manual Point Count*, ASTM E562 − 19, ASTM International, West Conshohocken, PA **2019**.

[29] ASTM, *Standard Test Methods for Determining Average Grain Size*, ASTM E112 − 13, ASTM International, West Conshohocken, PA **2013**.

[30] R. L. Higginson, C. M. Sellars, *Worked Examples in Quantitative Metallography*, Maney Publishing, Carlton House Terrace, London **2003**.

[31] M. Soliman, H. Palkowski, *Metall. Mater. Trans. A* **2008**, *39*, 2513.

[32] B. Aksakal, F. Karaca, R. Arikan, *Int. J. Mater. Res.* **2010**, *101*, 684.

[33] M. Delincé, Y. Bréchet, J. D. Embury, M. G. D. Geers, P. J. Jacques, T. Pardoen, *Acta Mater.* **2007**, *55*, 2337.

[34] J. Lin, *Fundamentals of Materials Modelling for Meals Processing Technology Theories and Applications*, Imperial College Press, London **2015**.

[35] D. H. Shin, K. T. Park, *Mater. Sci. Eng. A* **2005**, *410–411*, 299.

[36] J. R. Hollomon, *Trans. Metall. Soc. AIME* **1945**, *162*, 268.

[37] Y. Tomita, K. Okabagashi, *Metall. Trans. A* **1985**, *16*, 865.

[38] J. Lian, Z. Jiang, J. Liu, *Mater. Sci. Eng. A* **1991**, *147*, 55.

[39] Z. Jiang, J. Lian, J. Chen, *Mater. Sci. Technol.* **1992**, *8*, 1075.

[40] X. Zuo, Y. Chen, M. Wang, *Mater. Res.* **2012**, *15*, 915.

[41] V. Colla, M. De sanctis, A. Dimatteo, G. Lovicu, A. Solina, R. Valentini, *Metall. Mater. Trans. A* **2009**, *40*, 2557.

[42] D. A. Korzekwa, D. K. Matlock, G. Krauss, *Metall. Trans. A* **1984**, *15A*, 1221.

[43] F. H. Samuel, *Mater. Sci. Eng.* **1987**, *92*, L1.

[44] Z. Zhao, T. Tong, J. Liang, H. Yin, A. Zhao, D. Tang, *Mater. Sci. Eng. A* **2014**, *618*, 182.

[45] H. P. Shen, T. C. Lei, J. Z. Liu, *Mater. Sci. Technol.* **1986**, *2*, 28.

[46] P. Ludwik, *Elemente der technologishen mechanik*, Springer, Berlin **1909**.

[47] H. W. Swift, *J. Mech. Phys. Solids* **1952**, *1*, 1.

[48] C. Crussard, *Rev. Metall.* **1950**, *47*, 589.

[49] B. J. Jaoul, *Mech. Phys. Solids* **1957**, *5*, 95.

[50] R. E. Reed-Hill, W. R. Cribb, S. N. Monteiro, *Metall. Trans. A* **1973**, *4*, 2665.

[51] A. S. Podder, D. Bhattacharjee, R. K. Ray, *ISIJ Int.* **2007**, *47*, 1058.

[52] A. Kundu, D. P. Field, *Mater. Sci. Eng. A* **2016**, *667*, 435.

[53] T. Tanaka, M. Nishida, K. Hashiguchi, T. Kato, in *Structure and Properties of Dual-Phase Steels* (Eds.: R. A. Kot, J. W. Morris), The Metallurgical Society of AIME, New Orleans **1979**, pp. 221.

[54] A. Ramazani, S. Bruehl, T. Gerber, W. Bleck, U. Prahl, *Mater. Des.* **2014**, *57*, 479.

[55] K. Nakaoka, Y. Hosoya, M. Ohmura, A. Nishimoto, in *Structure and Properties of Dual-Phase Steels* (Eds.: R. A. Kot, J. W. Morris), The Metallurgical Society of AIME, New Orleans. pp. 330.

2000518 (15 of 15)